Development of a Method for Estimating Height from LiDAR Data

Chizuka Fujishima.[1*], Junichi Susaki.[2] and Yoshie Ishii.[3]

[1]Student, Graduate School of Engineering, Kyoto University, Japan

[2]Professor, Graduate School of Engineering, Kyoto University, Japan

[3]Assistant Professor, Graduate School of Engineering, Kyoto University, Japan

*fujishima.chizuka.24t@st.kyoto-u.ac.jp (*Corresponding author's email only)

Abstract: *Currently, optical satellites are mainly used to observe land cover and topography. They provide full-color image and high spatial resolution data, but some problems exist including limitation of high-precision use of 3D maps and potential errors of several meters in estimated ground heights under forest canopy. To address these issues, altimeter LiDAR satellites with full-waveform LiDAR are now being developed. Full-waveform LiDAR is the technology to continuously acquire reflected intensity of LiDAR and record it as a reflected waveform. In addition, coordinated observation of commercial small optical observation systems and altimeter LiDAR satellite is expected to enable the generation of most advanced 3D terrain information in the world. For the practical use of altimeter LiDAR satellites, this study develops a method to estimate tree height from 3D point cloud data. Based on the methods adopted in existing LiDAR missions that perform high-precision height measurements in forested areas, I propose a method to estimate tree height from reflected waveform created from point cloud data. Also, considering the correlation between waveform and point cloud data, I propose a method to estimate tree height directly from point cloud data. The feature of this study is applying the assumption that there are two types of point clouds -ground points and vegetation points- and they exist according to a separate distribution. The estimated heights are validated by comparing them to the true value. The minimum RMSE was 2.20 m for the waveform-based estimation and 0.31 m for the point cloud-based estimation. Especially in flat areas, most values could be estimated with an error of less than 1.00 m. In addition, the accuracy of point cloud separation and the features of the ground surface had a significant impact on the estimation accuracy. Future tasks are clarifying the relationship between the reflected waveform and point cloud data and developing a method for creating continuous maps with optical images through deep learning.*

Keywords: *Height estimation, LiDAR, Point cloud, Waveform*

Introduction

Currently, optical satellites are mainly used to observe land cover and topography. They provide full-color image and high spatial resolution data, but some problems exist including limitation of high-precision use of 3D maps and potential errors of several meters in estimated ground heights under forest canopy. To address these issues, altimeter LiDAR satellites with full-waveform LiDAR are now being developed. Full-waveform LiDAR is the technology to continuously acquire reflected intensity of LiDAR and record it as a reflected waveform. In addition, coordinated observation of commercial small optical observation systems and altimeter LiDAR satellite is expected to enable the generation of world's most advanced 3D terrain information. For the practical use of altimeter LiDAR

satellites, this study develops a method to estimate tree height from 3D point cloud data. We propose a method based on the principles adopted in existing LiDAR missions.

Existing LiDAR missions

a. ICESat-2:

Ice, Cloud, and land Elevation Satellite-2 (ICESat-2) is a satellite operated by National Aeronautics and Space Administration (NASA). The objectives are quantifying the polar ice mass balance, monitoring seasonal changes in ice sheets, tracking changes in ice sheet topography, estimating sea ice thickness, and measuring tree canopy height. A key feature of this mission is its ability to measure the height of ice sheets, clouds, and land areas using its onboard laser altimeter. However, because it is applying a photon-counting LiDAR specialized for ice sheet elevation measurement, it cannot perform high-precision measurements of the ground surface height under forest canopies.

b. MOLI:

Multi-sensing Observation Lidar and Imager (MOLI) is the world's first forest observation system that is simultaneously equipped with a LiDAR which features multiple footprints (laser measurement points) and an imager. Furthermore, the MOLI mission is Japan's first mission to demonstrate an earth observation LiDAR using the International Space Station (ISS) Kibo Exposed Facility. As the nation's first space-based LiDAR demonstration, it is an important mission for acquiring the foundational technology for future satellite LiDAR systems. A key feature of this mission is its attempt to solve the previous challenges of determining the laser footprint position and the limitation of acquiring LiDAR data only at the satellite's nadir by fusing data by utilizing its simultaneously equipped imager. Additionally, by applying this system to forest observation from space, the height of the tree is estimated from the difference in distance between the canopy and the ground. This system determines this distance by measuring the time it takes for an emitted laser pulse to be received. Although progress has been made toward achieving estimation accuracy of 3 meters, challenges remain for estimations using LiDAR observations. These include improving the accuracy of continuous canopy height observation data, expanding to continuous surface data, and solving the degradation of tree height estimation accuracy due to ground slope within the footprint.

c. GEDI:

Global Ecosystem Dynamics Investigation (GEDI) is an Earth observation LiDAR mission currently operated by the United States. Deployed to the International Space Station (ISS)

in 2018 for a two-year mission at first, but it has since been extended twice and continues to collect data. Furthermore, it is expected to make approximately 10 billion cloud-free observations during its nominal 24-month mission period. A key feature of this mission is its ability to generate a LiDAR waveform by recording the amount of laser energy reflected from plant structures (stems, branches, and leaves) at different heights above the ground and quantifying the vertical distribution of vegetation. From the waveform information, four types of structural information can be extracted: surface topography, canopy height, canopy cover, and vertical structure. GEDI's validation data is reported to have an accuracy of RMSE = 6.6 m, MAE = 4.45 m, and $R^2 = 0.62$, and there are some studies that attempt to create a high-precision global forest canopy height map by combining this data with other types of data.

Methodology

In this study, we proposed two new methods for estimating tree height from 3D point cloud data. First, we proposed a method to estimate tree height using the reflected waveform, based on the principles adopted in existing LiDAR missions. Next, we proposed a method to estimate tree height directly from the point cloud data considering the correlation between the reflected waveform and the point cloud data. Then, we verified the accuracy by comparing the estimated tree height values with true values to evaluate the effectiveness of the proposed methods. A key feature of this research is that we set the assumption that the point cloud data consists of two types -ground points and vegetation points- and that each follows a separate distribution. A flowchart of the method of this study is shown in Figure1.

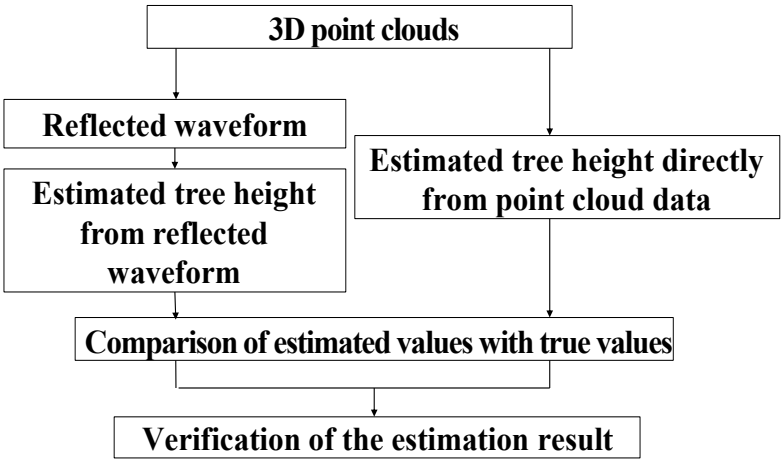

Figure 1: Overview of this study.

a. Estimation using the reflected waveform:

First, we calculated the point cloud density within a certain height range using the elevation information of the 3D point clouds. By creating a histogram that showed the point cloud density in each height range, we demonstrated the distribution of reflection intensity. Next, we approximated the created histogram to a Gaussian mixture model using the Expectation-maximization algorithm (EM algorithm) to calculate the initial values for each distribution. The EM algorithm is an algorithm for estimating the appropriate parameters of a probability distribution model using the maximum likelihood estimate, where the model's functional form is determined to fit the target data. Then, by using these initial values, we approximated the histogram to the waveform considering three types of distributions—Normal, Chi-squared, and Poisson. By fitting two types of probability distributions that approximated the low-height and non-low-height ranges of the histogram, respectively, and comparing the goodness of fit between the histogram and the probability distributions using Kullback-Leibler Divergence, we decided the separation point between the two probability distributions and classified the point clouds into two types, ground points and vegetation points, and a reflected waveform is finally created. A flowchart of the reflected waveform creation process is shown in Figure 2.

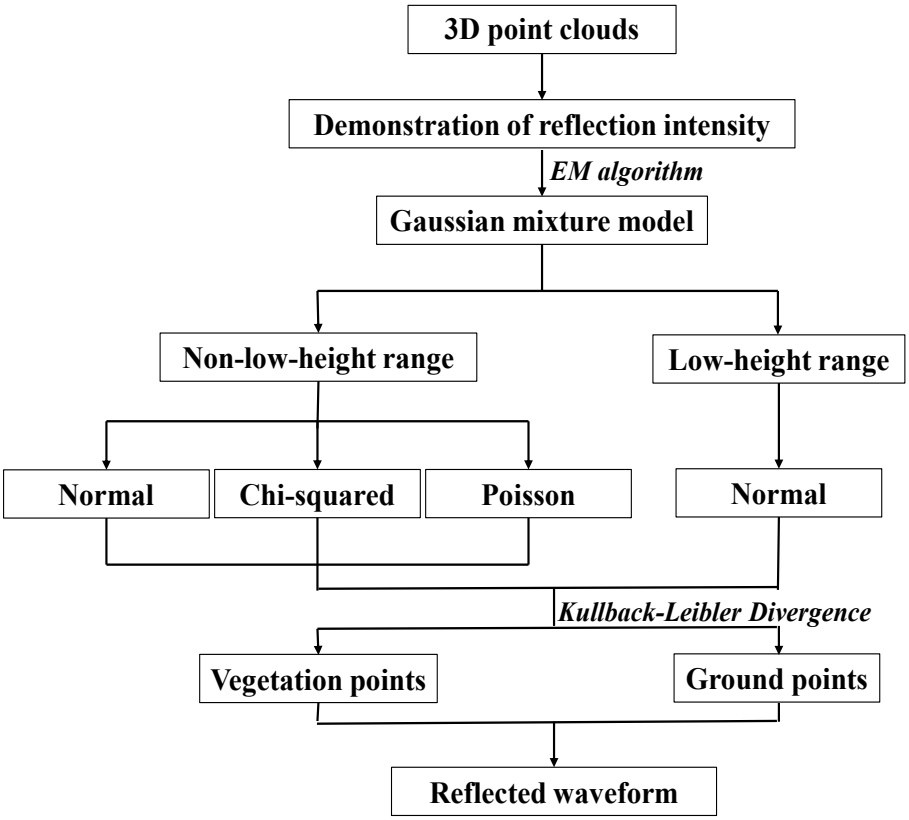

Figure 2: Reflected waveform creation process.

We considered the range with a height lower than the separation point, calculated with the method described above, as the ground domain, and the range with a higher height as the vegetation domain. Furthermore, we treated the waveform that approximated the histogram of the ground domain as the waveform from the ground point clouds, and the waveform that approximated the histogram of the vegetation domain as the waveform from the vegetation point clouds. As shown in Figure 3, The height at which the waveform from the ground point clouds reached its peak was regarded as the estimated ground height, S'.

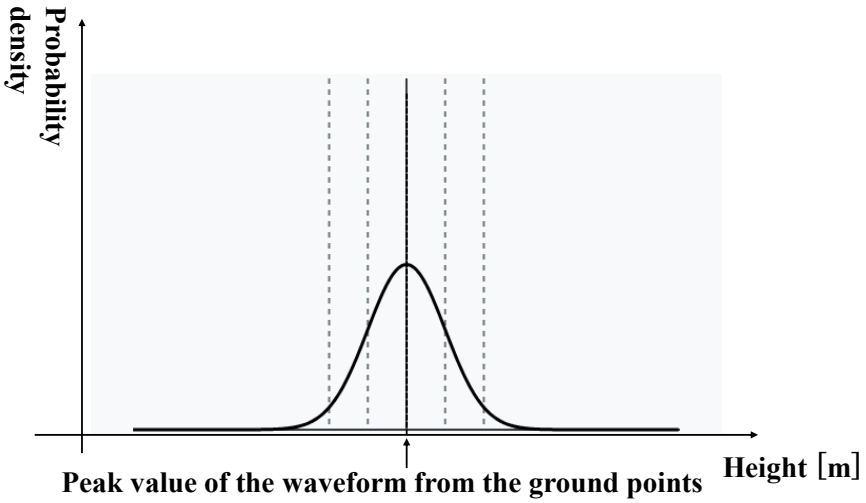

Figure 3: Method for estimating the ground height S'. The ground height is defined as the peak value of the waveform from the ground point clouds.

We defined the minimum value among the median value of each height range in the histogram as the estimated minimum ground height (S'_{min}), and the height of the separation point between the ground and vegetation domains as the estimated maximum ground height (S'_{max}). Additionally, the estimated mean ground height (S'_{mean}) and the estimated difference between the maximum and minimum ground height (S'_{height}) were defined using the following equations (1) and (2).

$$S'_{mean} = \frac{(S'_{max} + S'_{min})}{2} \quad (1)$$

$$S'_{height} = S'_{max} - S'_{min} \quad (2)$$

As shown in Figure 4, the height-converted average of the median values of each height region was regarded as the estimated canopy height, T'. These ranges contained all data points up to the position where the area surrounded by the reflected waveform from the vegetation point clouds reached the top 5% of the total surrounding area for the entire vegetation domain.

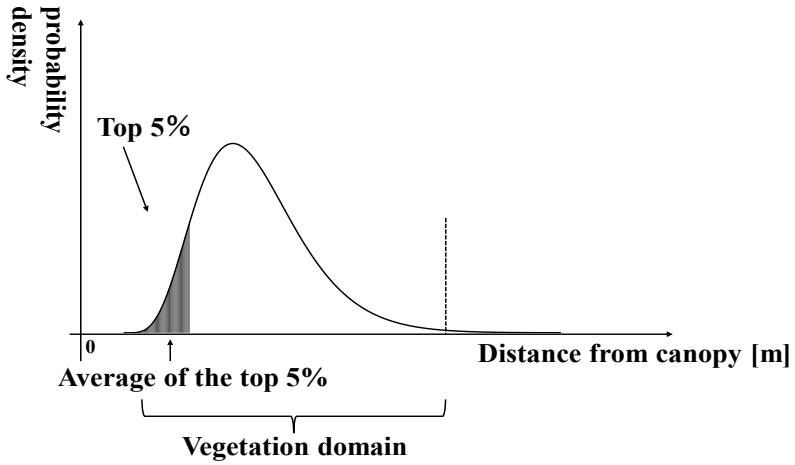

Figure 4: Method for estimating the canopy height T'. The canopy height is defined as the average height of the data belonging to the top 5% of the highest points within the vegetation point clouds.

We applied two approaches for calculating the estimated tree height: one using the estimated ground height, S', and another using the estimated mean ground height, S'_{mean}. The estimated tree height calculated using S' was defined as ST', and the estimated tree height calculated using S'_{mean} was defined as ST'_{mean}, following equations (3) and (4).

$$ST' = T' - S' \tag{3}$$

$$ST'_{mean} = T' - S'_{mean} \tag{4}$$

b. Estimation using the point cloud data directly:

By using a filtering process, we realized a method that can accurately classify the point clouds into two types, ground points and vegetation points with low calculation cost. The filtering process is a method for separating 3D coordinate point clouds into ground and non-ground data. First, x-y plane where point cloud data existed was divided into four equal-area grids to obtain the minimum height value in each grid. Next, the equation of a plane that passed through all these local minimum values was determined by finding the coefficients of the plane equation that minimized the sum of the squared distances between the plane and the minimum height values, its normal vector was calculated, and a threshold necessary for extracting the ground points was set. Finally, the estimated ground surface was updated using the set threshold, and the ground points were extracted.

We regarded the average height of all ground points, extracted by the filtering process, as the estimated ground height, S. Furthermore, we defined the minimum height among ground points as the estimated minimum ground height (S_{min}), and the maximum height among

ground points as the estimated maximum ground height (S_{max}). Additionally, the estimated mean ground height (S_{mean}) and the estimated difference between the maximum and minimum ground height (S_{height}) were defined using the following equations (5) and (6).

$$S_{mean} = \frac{(S_{max} + S_{min})}{2} \quad (5)$$

$$S_{height} = S_{max} - S_{min} \quad (6)$$

Points not extracted by the filtering process were considered as the vegetation point clouds. We regarded the average height of the data belonging to the top 5% of the highest points within the entire vegetation point clouds as the estimated canopy height, T. In this method, the estimated tree height**,** ST was defined following equation (7).

$$ST = T - S \quad (7)$$

Experiments

a. Study area:

In this study, we used 3D coordinate data provided by Shizuoka Prefecture as the aircraft LiDAR measurement data. This data is acquired based on the "VIRTUAL SHIZUOKA" initiative, which reproduces Shizuoka Prefecture in full scale within a virtual space using a vast point cloud data obtained by surveying the real world with high precision over a wide area using laser scanners and other equipment. This point cloud data contains 3D coordinate information (latitude, longitude, and elevation). Because it is measured by high-density airborne laser scanning that can measure the ground even in vegetated areas as far as the laser beam can reach, high-density data of 16 points/m² or more can be obtained. Furthermore, the data is released as open data from the G-spatial Information Center and is freely available to anyone under a Creative Commons license (CC-BY 4.0). For these reasons, we adopted the 3D coordinate data from Shizuoka Prefecture as the aircraft LiDAR data for this study. Additionally, Figure 5 shows an aerial photograph of Shizuoka Prefecture. The nine circles in the figure indicate the study sites. As the objective of this study is to develop a method for estimating ground and tree heights, 17 samples including vegetated areas were selected from all study sites.

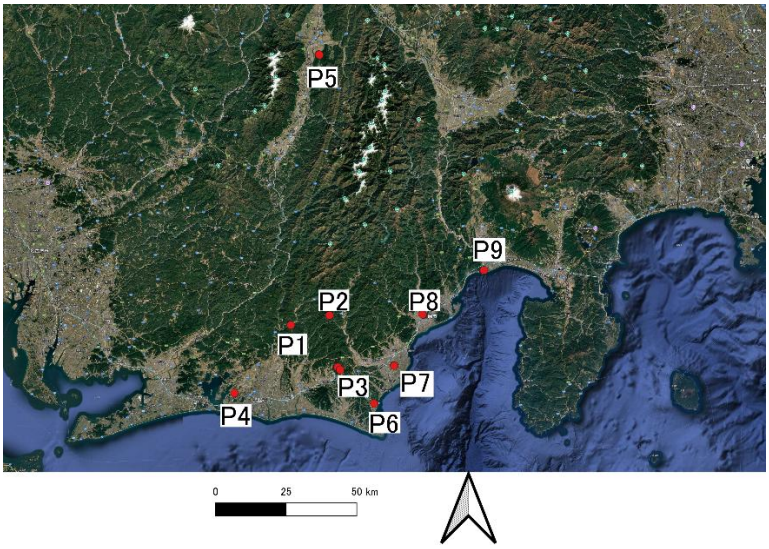

Source: Google Maps (Satellite View)

Figure 5: Study Area.

b. Point Cloud Dataset:

In this study, we used point cloud datasets extracted from each of the study sites P1 through P9, shown in Figure 5. These datasets were created by clipping the area where the x and y coordinate values were within a 12-meter diameter circle on the x-y plane. The relationship between the study sites and the point cloud datasets is summarized in Table 1.

Table 1: Relationship between study sites and clipped point cloud datasets.

	P1	**P2**	**P3**
Point cloud datasets	T1, T2	T3, T4	T5, T6, T7
	P4	**P5**	**P6**
Point cloud datasets	T8	T9, T10	T11
	P7	**P8**	**P9**
Point cloud datasets	T12, T13	T14, T15	T16, T17

Furthermore, Figure 6 shows the distribution of each point cloud dataset when viewed from three directions, in order from left to right: directly above, directly besides, and diagonally.

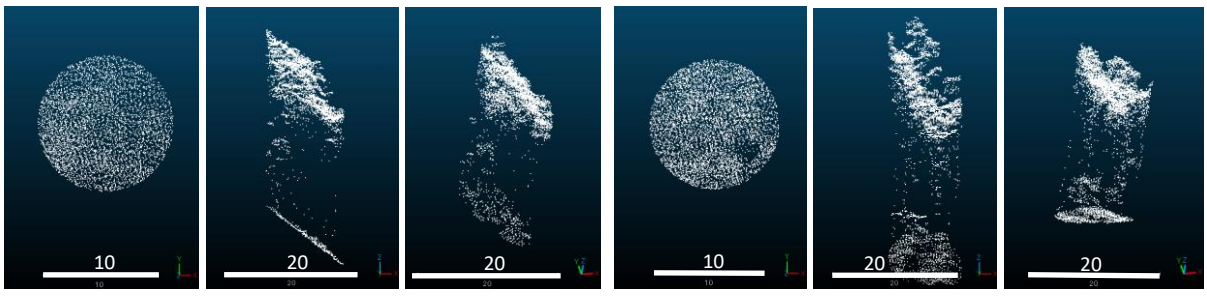

T1 T2

Source: VIRTUAL SHIZUOKA

Figure 6: Distribution of each point cloud dataset. (*cont.*)

(left: above, middle: beside, right: diagonally)

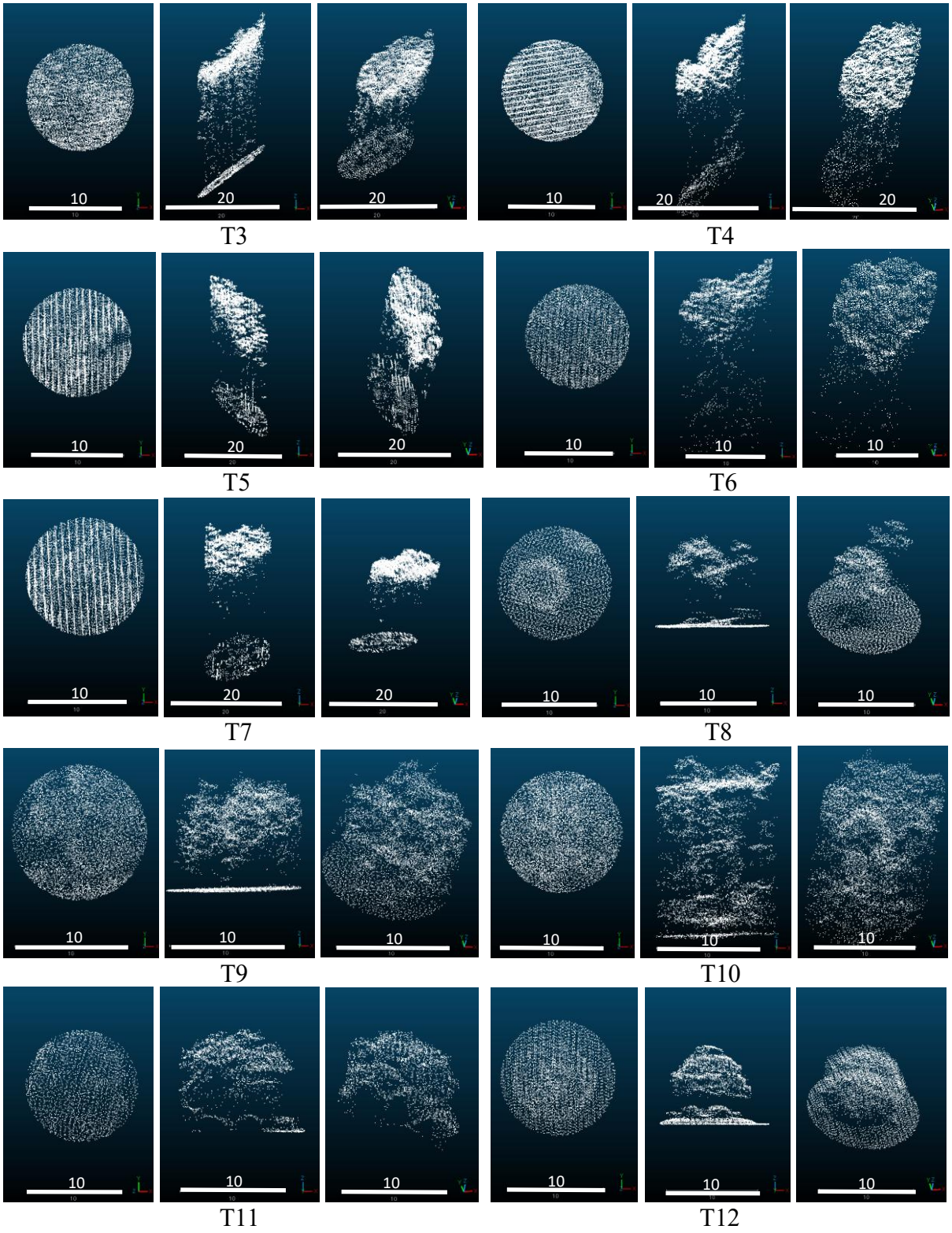

Source: VIRTUAL SHIZUOKA

Figure 6: Distribution of each point cloud dataset. (*cont.*)

(left: above, middle: beside, right: diagonally)

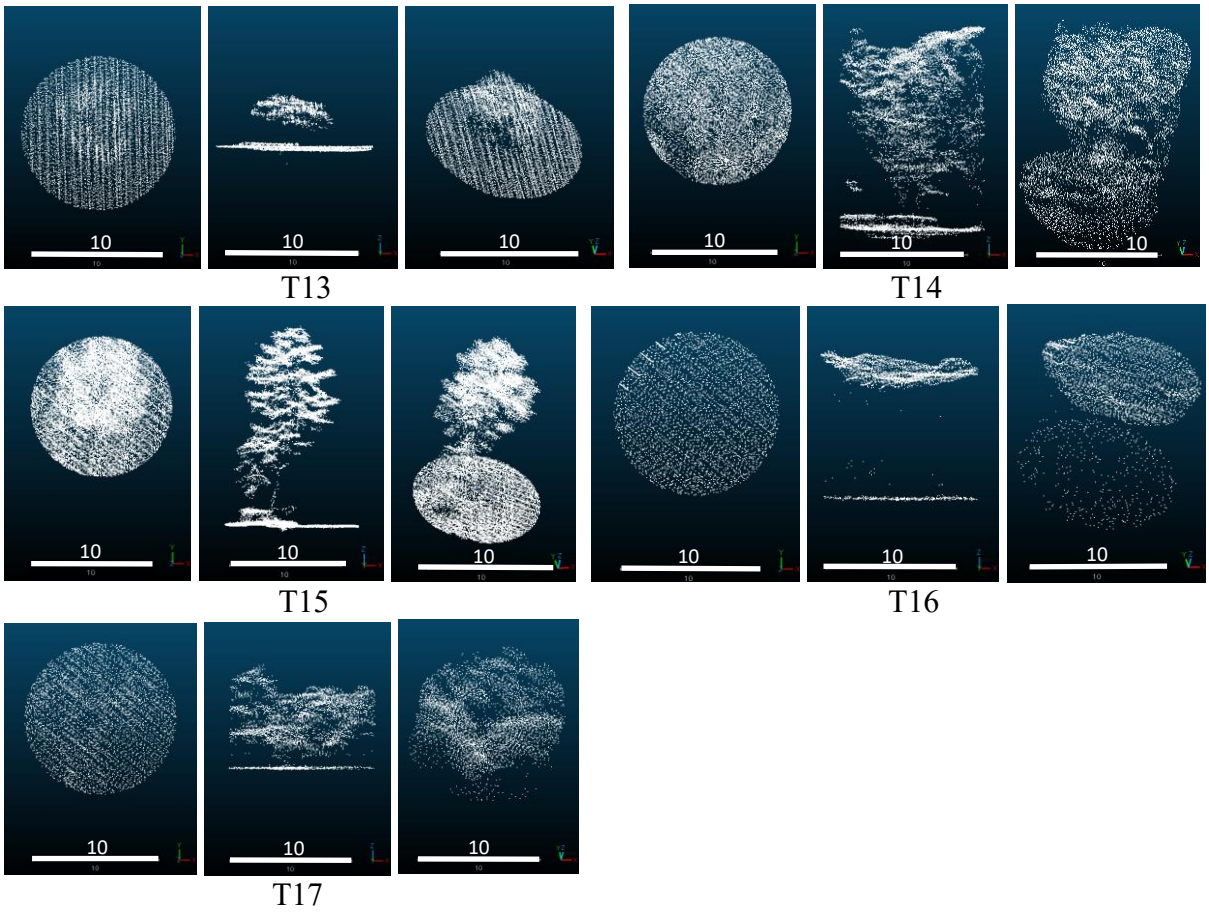

Source: VIRTUAL SHIZUOKA

Figure 6: Distribution of each point cloud dataset. (*cont.*)

(left: above, middle: beside, right: diagonally)

c. Verification datasets:

In this study, we concluded that accuracy verification could be possible by treating the results of highly accurate estimation as equivalent to true values. This was done after classifying the point cloud data into ground points and vegetation points by visually checking its distribution. We judged points concentrated in the low-height range as the ground point clouds. We regarded the average height of all ground points as the true ground height, $\overline{S}$. Furthermore, we defined the minimum height among ground points as the true minimum ground height ($\overline{S}_{\text{min}}$), and the maximum height among ground points as the true maximum ground height ($\overline{S}_{\text{max}}$). Additionally, the true mean ground height ($\overline{S}_{\text{mean}}$) and the true difference between the maximum and minimum ground height ($\overline{S}_{\text{height}}$) were defined using the following equations (8) and (9).

$$\overline{S}_{mean} = \frac{(\overline{S}_{max} + \overline{S}_{min})}{2} \quad (8)$$

$$\overline{S}_{height} = \overline{S}_{max} - \overline{S}_{min} \quad (9)$$

Points not extracted as the ground point clouds were considered as the vegetation point clouds. We regarded the average height of the data belonging to the top 5% of the highest points within the entire vegetation point clouds as the true canopy height, $\overline{T}$. In this method, the true tree height, $\overline{ST}$ was defined following equation (10).

$$\overline{ST} = \overline{T} - \overline{S} \quad (10)$$

d. Estimation using the reflected waveform:

Figure 7 shows the best fitting probability distribution, overlaid on the histogram. It also separately displays the probability distribution approximating the low-altitude range of the histogram (blue) and the distribution approximating the non-low-altitude range (green). Furthermore, the mean value of each probability distribution, calculated via EM algorithm, is shown as a dotted line, and the calculated separation point between the low and non-low altitude ranges is indicated by a red line. This figure confirms that the distribution of reflection intensity, as estimated from the 3D coordinate data, is simulated with high accuracy.

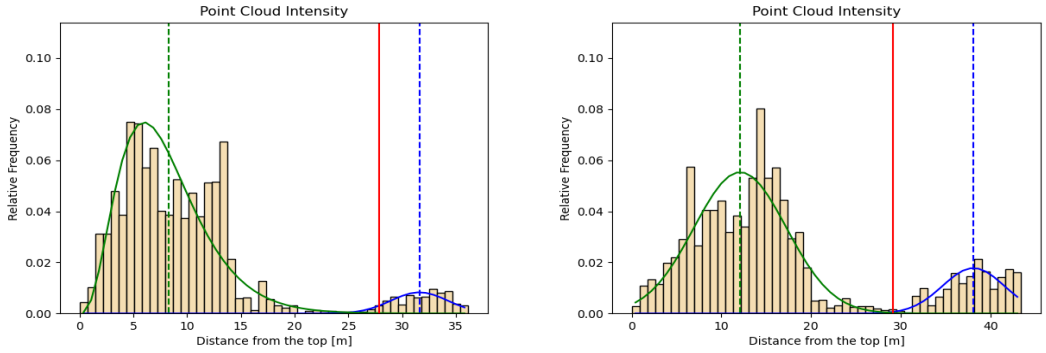

T1 T2

Figure 7: A histogram showing point cloud density at different height ranges, with the best fitting probability distribution overlaid on the histogram. (*cont.*)

(blue : fitted probability distributions for the low-range, green: fitted probability distributions for the non-low-range, solid line: distribution, dotted line: mean value of each distribution, red: separation point between two ranges)

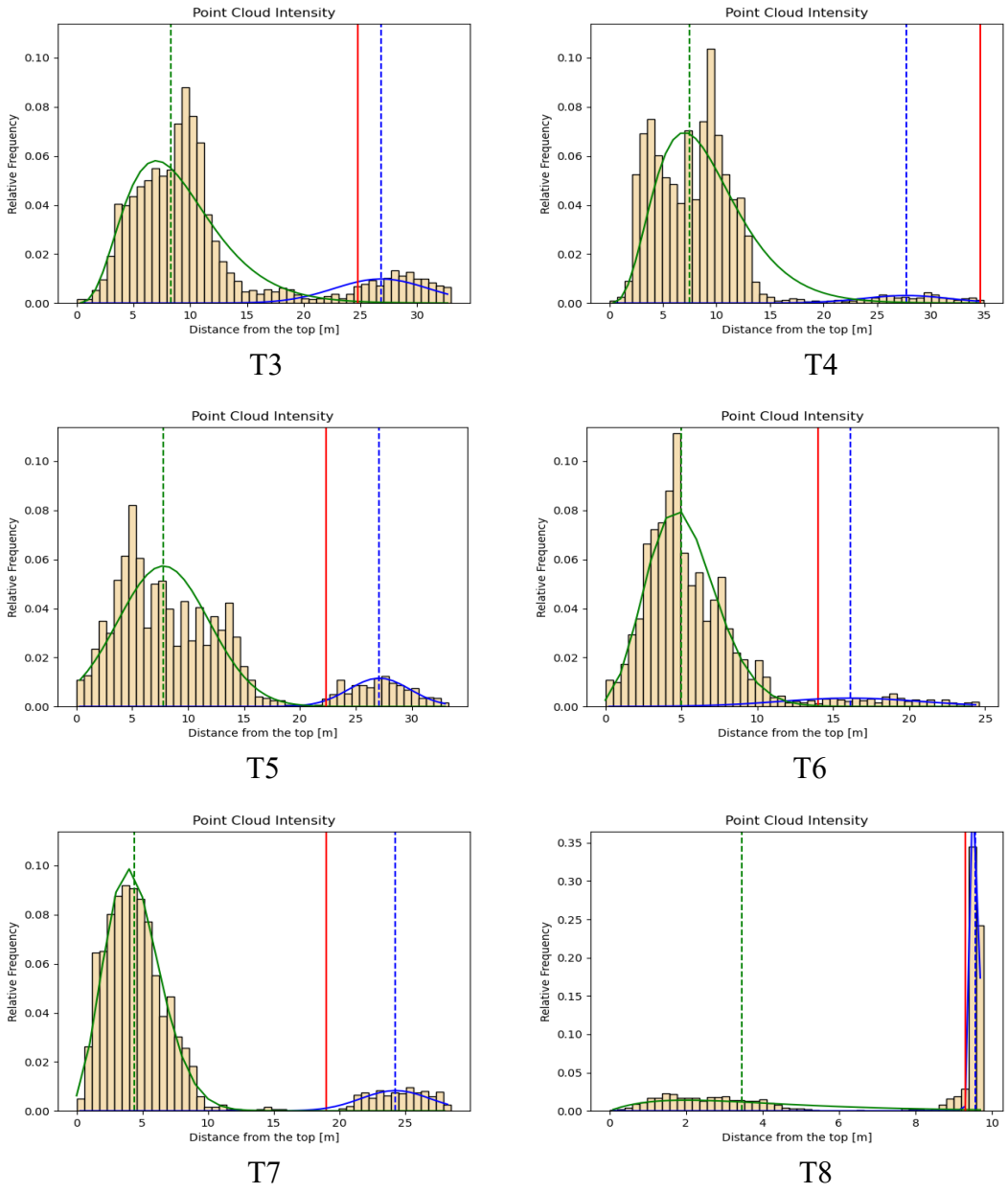

Figure 7: A histogram showing point cloud density at different height ranges, with the best fitting probability distribution overlaid on the histogram. (*cont.*)

(blue : fitted probability distributions for the low-range, green: fitted probability distributions for the non-low-range, solid line: distribution, dotted line: mean value of each distribution, red: separation point between two ranges)

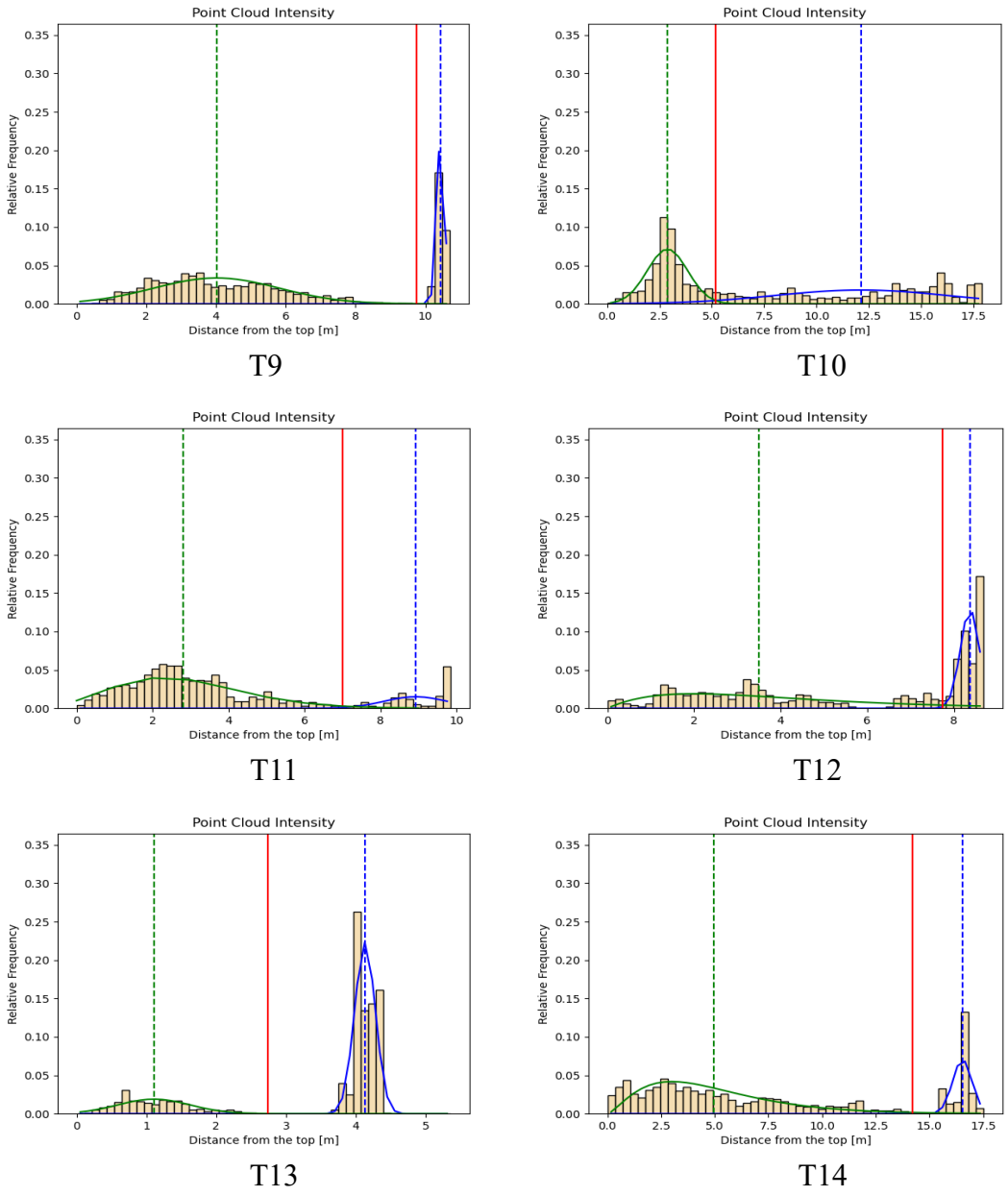

Figure 7: A histogram showing point cloud density at different height ranges, with the best fitting probability distribution overlaid on the histogram. (*cont.*)

(blue : fitted probability distributions for the low-range, green: fitted probability distributions for the non-low-range, solid line: distribution, dotted line: mean value of each distribution, red: separation point between two ranges)

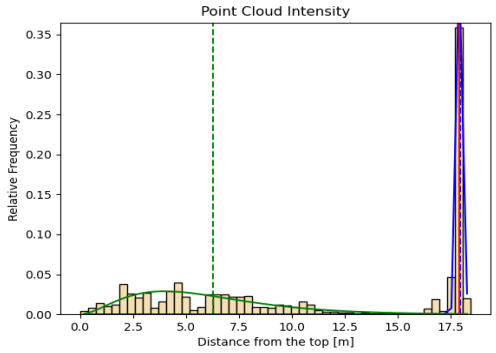

T15

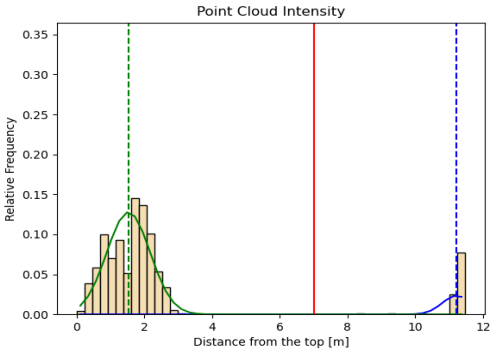

T16

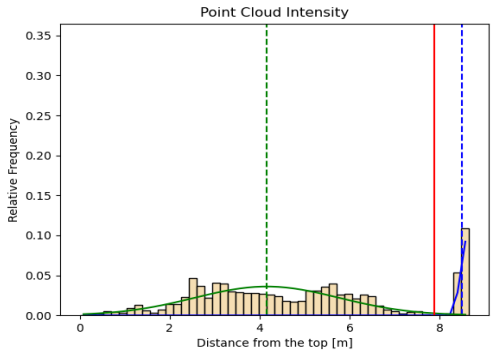

T17

Figure 7: A histogram showing point cloud density at different height ranges, with the best fitting probability distribution overlaid on the histogram. (*cont.*)

(blue : fitted probability distributions for the low-range, green: fitted probability distributions for the non-low-range, solid line: distribution, dotted line: mean value of each distribution, red: separation point between two ranges)

The estimated tree heights, ST' and ST'$_{mean}$, calculated for each point cloud dataset are summarized in Table 2. The true tree height calculated for each dataset is also shown alongside for comparison.

Table 2: Estimated tree heights using the reflected waveform, with corresponding true values estimated from verification datasets and errors.

(a) Tree height is from ST'

	Estimated value	True value	Error	Estimated value	True value	Error
	T1			**T2**		
Tree height (m)	29.29	30.42	-1.13	35.09	37.42	-2.33
	T3			**T4**		
Tree height (m)	24.20	26.11	-1.91	31.95	26.87	5.08
	T5			**T6**		
Tree height (m)	25.86	26.21	-0.35	15.17	19.06	-3.89
	T7			**T8**		
Tree height (m)	23.42	23.66	-0.24	9.12	8.93	0.19
	T9			**T10**		
Tree height (m)	9.61	9.35	0.26	10.97	16.49	-5.52
	T11			**T12**		
Tree height (m)	8.96	9.26	-0.30	7.99	8.16	-0.17
	T13			**T14**		
Tree height (m)	3.94	3.85	0.09	15.95	16.43	-0.48
	T15			**T16**		
Tree height (m)	16.86	17.20	-0.34	10.87	10.97	-0.10
	T17					
Tree height (m)	7.56	7.50	0.06			

(b) Tree height is from ST'_{mean}

	Estimated value	True value	Error	Estimated value	True value	Error
	T1			**T2**		
Tree height (m)	29.65	30.42	-0.77	33.35	37.42	-4.07
	T3			**T4**		
Tree height (m)	26.18	26.11	0.07	31.95	26.87	5.08
	T5			**T6**		
Tree height (m)	26.52	26.21	0.31	18.35	19.06	-0.71
	T7			**T8**		
Tree height (m)	22.80	23.66	-0.86	9.12	8.93	0.19
	T9			**T10**		
Tree height (m)	9.40	9.35	0.05	10.44	16.49	-6.05
	T11			**T12**		
Tree height (m)	8.38	9.26	-0.88	7.73	8.16	-0.43
	T13			**T14**		
Tree height (m)	3.83	3.85	-0.02	15.07	16.43	-1.36
	T15			**T16**		
Tree height (m)	17.05	17.20	-0.15	8.91	10.97	-2.06
	T17					
Tree height (m)	7.21	7.50	-0.29			

e. Estimation using the point cloud data directly:

The estimated tree height, ST, calculated for each point cloud dataset is summarized in Table 3. The true tree height calculated for each dataset is also shown alongside for comparison.

Table 3: Estimated tree heights using the point cloud data, with corresponding true values estimated from verification datasets and errors.

	Estimated value	True value	Error	Estimated value	True value	Error
	T1			**T2**		
Tree height (m)	30.44	30.42	0.02	37.28	37.42	-0.14
	T3			**T4**		
Tree height (m)	26.00	26.11	-0.11	26.70	26.87	-0.17
	T5			**T6**		
Tree height (m)	26.11	26.21	-0.10	17.95	19.06	-1.11
	T7			**T8**		
Tree height (m)	23.64	23.66	-0.02	8.94	8.93	0.01
	T9			**T10**		
Tree height (m)	9.35	9.35	0.00	16.47	16.49	-0.02
	T11			**T12**		
Tree height (m)	8.93	9.26	-0.33	8.13	8.16	-0.03
	T13			**T14**		
Tree height (m)	3.84	3.85	-0.01	16.88	16.43	0.45
	T15			**T16**		
Tree height (m)	17.16	17.20	-0.04	10.97	10.97	0.00
	T17					
Tree height (m)	7.53	7.50	0.03			

Results

a. Estimation using the reflected waveform:

For each point cloud dataset, the estimated tree heights, ST' and ST'$_{mean}$, calculated using the reflected waveform, were compared with the true tree height, $\overline{ST}$. The corresponding scatter plots are shown in Figure 8. Furthermore, the ideal line, which the data should follow if the estimated values are equal to the true values, is overlaid on the plots. About overall accuracy, the RMSE was 2.20 m for ST' and 2.28 m for ST'$_{mean}$. This indicates that using ST' as the estimated tree height resulted in less dispersion and a better estimation. Therefore, this indicates that when estimating tree height using the reflected waveform, a more accurate estimation can be achieved by adopting S'- the height at which the waveform from the ground point clouds reaches its peak - as the estimated ground height.

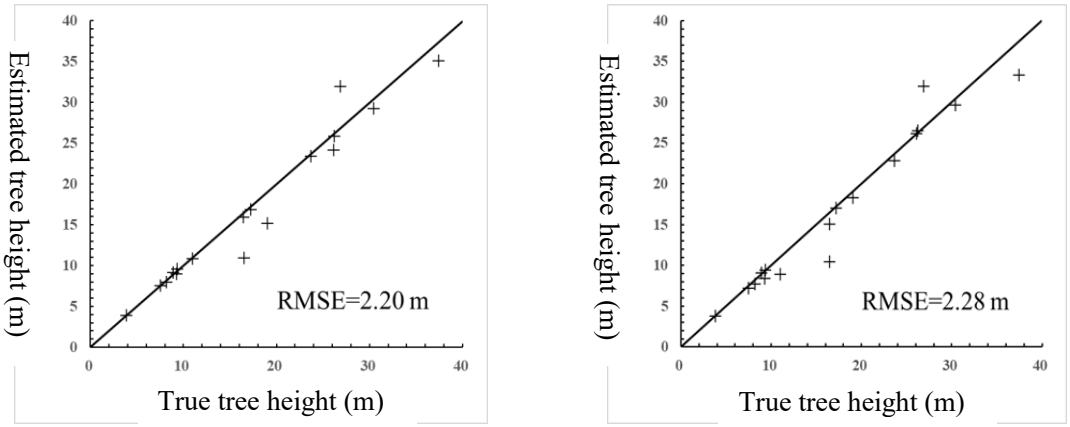

(a) Tree height is from ST' (b) Tree height is from ST'_{mean}

Figure 8: Accuracy of estimation using the reflected waveform. The estimated tree heights are compared with the true tree heights. The line is that the data should follow when the estimated and true values are the same.

For each point cloud dataset, the relative error was calculated by comparing the estimated tree height, ST' with the true tree height, $\overline{ST}$. The distribution of this error is shown in Figure 9.

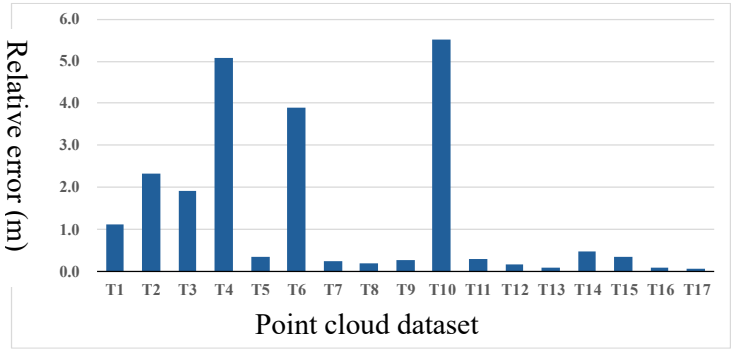

Figure 9: Relative errors of estimation using the reflected waveform.

b. Estimation using the point cloud data directly:

For each point cloud dataset, the estimated tree height, ST, calculated using the point cloud data directly, was compared with the true tree height, $\overline{ST}$. The corresponding scatter plot is shown in Figure 10. Furthermore, the ideal line, which the data should follow if the estimated values are equal to the true values, is overlaid on the plot. About overall accuracy, the RMSE was 0.31 m, which indicates that it is a very good estimation result.

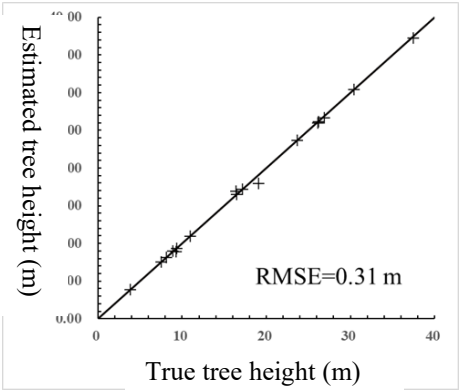

Figure 10: Accuracy of estimation using the point cloud data directly. The estimated tree heights are compared with the true tree heights. The line is that the data should follow when the estimated and true values are the same.

For each point cloud dataset, the relative error was calculated by comparing the estimated tree height, ST' with the true tree height, $\overline{ST}$. The distribution of this error is shown in Figure 11.

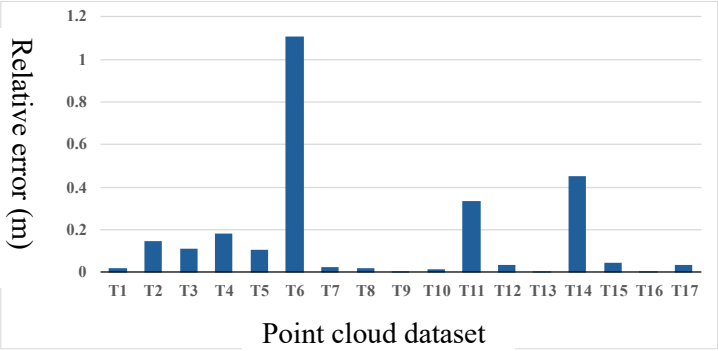

Figure 11: Relative errors of estimation using the point cloud data directly.

Discussion

From the distribution of each point cloud dataset shown in Figure 6, datasets T1 through T7 can be confirmed that the ground surface slope is steep, and the points in the ground region are distributed diagonally across a wide range of heights. On the other hand, datasets T8 through T17 can be confirmed that the ground surface slope is gentle, and the points in the ground region are concentrated within a certain range of heights. In other words, the point cloud dataset used in this study can be classified into two groups: T8 through T17, which were acquired at areas with relatively flat ground surfaces, and T1 through T7, which were acquired at areas with relatively sloped ground surfaces.

a. Sloped ground surfaces:

According to Figure 9, among the datasets T1 through T7, which were acquired at areas with relatively sloped ground surfaces, the tree height estimation error was within 1.00 m for two datasets, T5 and T7. On the other hand, for two other datasets, T4 and T6, the tree height estimation error exceeded 3.00 m. Since the MOLI mission aims to achieve a tree height accuracy of 3.00 m, it can be said that while a high-precision estimation was possible for the former group, it was not achieved for the latter. Furthermore, according to Figure 11, high-precision estimation with an error of less than 1.00 m was possible for all datasets except T6. In this study, since the datasets T1 through T7 were all acquired in forested areas, we assume that effects of undergrowth exist all sites. We consider that the spread of the point cloud density distribution in the low-height range affects the classification accuracy between ground and vegetation points, which in turn appear as the difference in estimation accuracy. Specifically, at sites where only a few points are detected near the ground surface, the distribution from ground points does not appear clearly. This will lead to misjudge the ground point distribution as spread over a wide area, making a precise separation between ground and vegetation points difficult. Furthermore, at sites where many points are detected near the ground surface, many points from undergrowth near the ground are also detected. This will similarly make a precise separation between ground and vegetation points difficult.

b. Flat ground surfaces:

According to Figure 9, among the datasets T8 through T17, which were acquired at areas with relatively flat ground surfaces, high-precision estimation with an error of less than 1.00 m was possible for all datasets except T10. Furthermore, according to Figure 11, high-precision estimation was possible for all these datasets. In this case, only the T10 did not show a clear peak in the low-height range that seemed to be attributed to the ground points. We consider that this appears to be the difference in estimation accuracy. We also consider the effects of undergrowth as the reason for the absence of a peak in T10. We assume that in areas with dense undergrowth, as many points as the ground points appear near the ground surface. This will lead to misjudge the ground point distribution as spread over a wide area, making a precise separation between ground and vegetation points difficult. In other words, for areas with flat ground surfaces, high-precision estimation is possible using either the waveform or the point cloud data, if the effects of undergrowth are small. On the other hand, in areas with significant undergrowth, achieving high-precision estimation becomes difficult when using the waveform-based method.

Conclusions

In this study, we developed a method to estimate tree height from 3D point cloud data. We proposed two types of tree height estimation methods: one was from reflected waveforms, and another was directly from point cloud data. It was shown that estimation using the point cloud data directly could achieve a more accurate estimation. Furthermore, it was confirmed that the accuracy of the separation between ground and vegetation points had a large impact on the tree height estimation. As shown in Figure 12, The estimation accuracy differs depending on various conditions. For sites with sloped ground and undergrowth, high-precision estimation was possible when the accuracy of the separation was high, and it could not be achieved when the accuracy of it was low. In addition, for sites with flat ground, high-precision estimation was possible without undergrowth, and it could not be achieved with undergrowth.

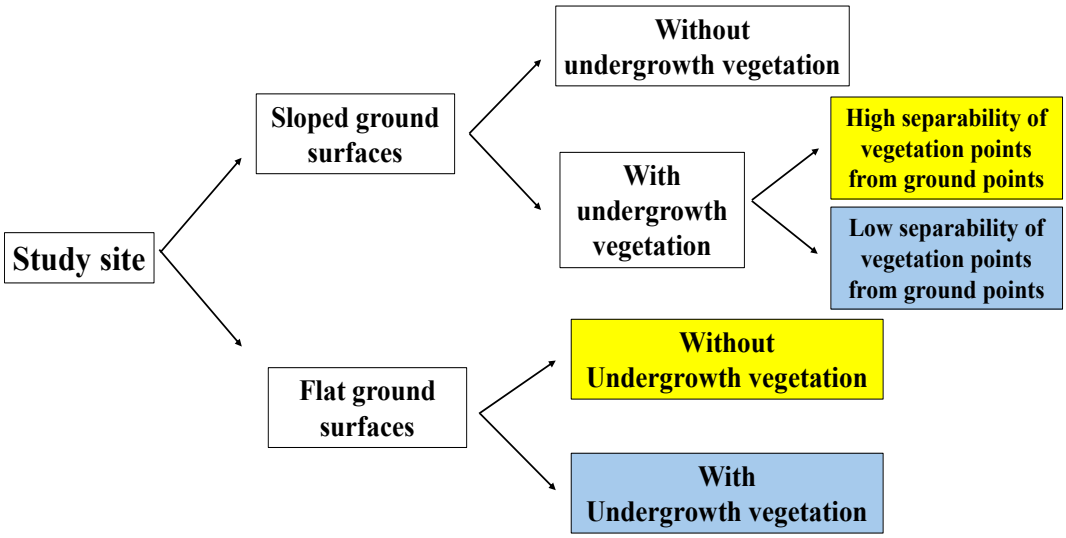

Figure 12: the estimation accuracy and conditions.
(yellow: high accuracy, blue: low accuracy, white: unjudgeable)

For future work, it will be necessary to consider the application to altimeter LiDAR satellites. For example, clarifying the relationship between the reflected waveform and point cloud data, and developing a method for acquiring continuous height information.

References

Potapov, P., (2021). Mapping global forest canopy height through integration of GEDI and Landsat data. *Remote Sensing of Environment, Volume 253-2021, pp. 112165*

Sugimoto, N., (2023). Designing the Future Cities Using a Digital Twin -VIRTUAL SHIZUOKA PROJECT-. *Transactions on AI and Data Science, Volume 4-2023, No. 2*

Susaki, J., (2012). Adaptive Slope Filtering of Airborne LiDAR Data in Urban Areas for Digital Terrain Model (DTM) Generation. *Remote Sensing, Volume 4-2012, No. 6*

Reference to an article in online journals or online first [DOI]:

Okawa, Y., Sakaizawa, D., Mitsuhashi, R., Sawada, Y., Imai, T., & Sumita, T. (2021). Overview and progress of the ISS-borne LiDAR demonstration MOLI: The Laser Society of Japan. https://laser-sensing.jp/41stLSS/41st_papers/LSS41_B4_okawa.pdf

Reference to a book (ISBN):

Junichi Susaki & Michinori Hatayama, (2013), Geoinformatics.

For published conference proceedings:

Suyama, K., Funabora, Y., Doki, S., & Doki, K. (2015). Robust Improvement of Localization Using Particle Filter by Sensor Fusion Method Based on KL-Divergence. *The 2015 JSME Robotics and Mechatronics Conference, 17-19 May 2015, Kyoto, Japan*.

For Internet resources:

Allison Corporation. (n.d.). Gaussian Mixture Model (GMM) and EM Algorithm. Retrieved February 7, 2025, from https://www.allisone.co.jp/html/Notes/Mathematics/statistics/gmm/index.html

NASA. (n.d.). GEDI. Retrieved February 7, 2025, from https://gedi.umd.edu/instrument/instrument-overview/

Remote Sensing Technology Center of Japan. (n.d.). ICESat-2. Retrieved February 7, 2025, from https://www.restec.or.jp/satellite/icesat-2.html

SPACE SHIFT.com. (n.d.). the difference between optical and SAR satellites. Retrieved February 7, 2025, from https://www.spcsft.com/technology/satellites/

The Laser Sensing Society of Japan. (n.d.). Mission of tree crown height measurement: Multi-footprint Observation LIdar (MOLI). Retrieved February 8, 2025, from https://laser-sensing.jp/31thLSS/31th_papers/21_P-7_Sakaizawa.pdf